JGR Solid Earth

RESEARCH ARTICLE
10.1029/2023JB027869

Scaling Laws for Mixed Heated Convection With Pseudoplastic Rheology: Implications for the Bistability of Tectonic Mode

Amy L. Ferrick[1] **and Jun Korenaga**[1]

[1]Department of Earth and Planetary Sciences, Yale University, New Haven, CT, USA

Key Points:

- Mantle convection scaling laws are generalized for the heating mode and rheology appropriate for planetary mantles
- Convective properties may be accurately predicted for both the plate tectonic and stagnant lid modes of convection
- Tectonic mode is unique for a given rheological scenario, despite the apparent bistability of numerical simulations

Supporting Information:

Supporting Information may be found in the online version of this article.

Correspondence to:

A. L. Ferrick,
amy.ferrick@yale.edu

Citation:

Ferrick, A. L., & Korenaga, J. (2023). Scaling laws for mixed heated convection with pseudoplastic rheology: Implications for the bistability of tectonic mode. *Journal of Geophysical Research: Solid Earth*, *128*, e2023JB027869. https://doi.org/10.1029/2023JB027869

Received 15 SEP 2023
Accepted 2 NOV 2023

Author Contributions:

Conceptualization: Amy L. Ferrick, Jun Korenaga
Formal analysis: Amy L. Ferrick
Investigation: Amy L. Ferrick
Methodology: Amy L. Ferrick, Jun Korenaga
Supervision: Jun Korenaga
Visualization: Amy L. Ferrick
Writing – original draft: Amy L. Ferrick
Writing – review & editing: Amy L. Ferrick, Jun Korenaga

Abstract Plate tectonics is a tectonic style thought to be the hallmark of habitable planets, and yet the inherent complexities of plate tectonic convection have clouded the establishment of simple scaling laws with which to model convective behavior and thermal evolution. We have recently developed a scaling approach for mixed heated convection, based upon several simple physical principles. Here, we generalize our scaling approach to mixed heated convection with pseudoplastic rheology, which gives rise to the plate tectonic mode of convection. We then apply our scaling results to the so-called bistability of tectonic mode. By illustrating common pitfalls regarding heating mode and nondimensionalization, we demonstrate that tectonic mode is unique with respect to key planetary properties, and that a convective regime diagram for terrestrial planets is within reach.

Plain Language Summary Convection within planetary mantles (the rocky layer bounded by a thin crust and a metallic core) is driven by heating from within and from below, and it is largely dependent on rheology—how mantle rocks deform. We generalize convection scaling laws to the rheology and heating mode appropriate for planetary mantles. These scaling laws describe convective properties of plate tectonic convection, in which the surface layer of the mantle is weak enough to participate in convection, as well as stagnant lid convection, in which the surface layer is strong and immobile. We show that the state of the surface layer (the so-called tectonic mode) is unique for a given rheological scenario. This restores confidence in the prospect of predicting tectonic mode from first-order planetary properties, a crucial task given the connection between tectonic mode and habitability.

1. Introduction

Constraining the conditions for plate tectonics is one of the most outstanding problems in Earth and planetary sciences, especially in light of the connection between plate tectonics and habitability. Earth is apparently unique in having plate tectonics, wherein lithosphere can become sufficiently weak to participate in convection. All other terrestrial planets in the solar system are thought to experience stagnant lid convection (or at least prolonged periods of lid inactivity). On these planets, the lithosphere is too strong to deform significantly.

We must largely rely on modeling and theory to describe the different modes of mantle convection and the conditions required by each, as observations pertaining to tectonic mode are limited. However, convection of planetary mantles is inherently complex, and issues such as rheology and heating mode have prevented a definitive theoretical description of how convecting mantles behave (e.g., Choblet, 2012; Christensen, 1985; Foley & Bercovici, 2014; Gurnis, 1989; Korenaga, 2020; Lourenço et al., 2016). In terms of scaling theory for mantle convection, it is essential to generalize to the mixed heated mode, as planetary mantles are heated from within (due to radiogenic heat production, secular cooling, and tidal heating) and from below (due to core cooling). Recently, we have developed a scaling approach for mixed heated mantle convection (Ferrick & Korenaga, 2023), which we applied to convection with temperature-dependent viscosity. Full generality to planetary mantles requires additionally accounting for the brittle strength of the lithosphere, often emulated by the use of so-called pseudoplastic rheology, which allows for plate tectonic convection in numerical experiments. Alternative approaches to simulating plate tectonic convection include prescribing surface motion (e.g., Lowman et al., 2001; Monnereau & Quéré, 2001; Zhong et al., 2000) and implementing a strain-rate weakening rheology (e.g., Bercovici, 1993; Tackley, 1998). Pseudoplastic rheology has the advantage of producing self-consistent plate-like behavior via a relatively simple numerical implementation. Scaling laws for plate tectonic convection, either with pseudoplastic rheology (e.g., Grigné et al., 2005; Korenaga, 2010b; Wong & Solomatov, 2015) or otherwise (e.g., Foley &

Bercovici, 2014), have been derived either for purely internal or purely basal heating, but no such scaling laws exist for mixed heated convection.

In addition, to predict the behavior of mantle convection and the associated tectonic modes using scaling theory, an essential task is to construct the convection mode regime diagram: a prediction of tectonic mode as a function of planetary properties. Efforts within the past few decades toward predicting tectonic mode have reached conflicting conclusions about the role of factors such as planet size, heating mode, and surface conditions (e.g., Korenaga, 2010a; O'Neill & Lenardic, 2007; Stein et al., 2011; Valencia et al., 2007; Valencia & O'Connell, 2009; Van Heck & Tackley, 2011). For example, several studies concluded that the likelihood of plate tectonics increases with increasing planet size (Valencia et al., 2007; Valencia & O'Connell, 2009), whereas others reached the opposite conclusion (O'Neill & Lenardic, 2007; Stein et al., 2011). Van Heck and Tackley (2011) argued that the role of planet size depends on heating mode, and Korenaga (2010a) argued that, instead of planet size, the presence of surface water is most important for tectonic mode. Some studies proposed that these diverse and in some cases opposing results emerge from a history-dependence of tectonic mode (e.g., Noack & Breuer, 2014; Weller & Lenardic, 2012). For example, Weller and Lenardic (2012) found that numerical simulations with the same model parameters lead to different tectonic modes—either plate tectonic convection or stagnant lid convection—depending on whether the brittle yield stress has been increasing or decreasing. As a result, it has been proposed that tectonic mode is sensitive to small perturbations and commonly fluctuates (Lenardic et al., 2016; O'Neill et al., 2016), implying that detailed knowledge of a planet's evolution is required to predict tectonic mode. This poses a major challenge for the prediction of tectonic mode from first-order planetary observables.

In the following, we present scaling laws for mixed heated convection with pseudoplastic rheology, following the scaling approach of Ferrick and Korenaga (2023). Rather than phenomenological methods, this approach is based on fundamental physical properties of convection, which facilitates a relatively straightforward application to various rheological scenarios. These scaling laws allow for the solution of the heat flow and temperature structure of a convecting fluid with pseudoplastic rheology as a function of the intrinsic convective parameters. Using our scaling analysis, we show that plate tectonic convection and stagnant lid convection exhibit different first-order characteristics such as surface heat flow, internal temperature, and lithospheric viscosity contrast, even when the (nondimensional) model parameters are identical. This resolves a supposed barrier to predicting tectonic based on first-order planetary properties.

The structure of the paper is as follows: We first describe the theoretical formulation of convection with pseudoplastic rheology and temperature-dependent viscosity. Next, we derive scaling laws for such convection and test them with numerical simulations. We then apply our scaling approach to the bistability of convection within numerical simulations, and we discuss these results in the context of tectonic mode of terrestrial planets. Finally, we discuss implications for the fundamental task of predicting tectonic regime and suggest future work toward completing the description of convection with pseudoplastic rheology.

2. Theoretical Formulation

2.1. Rheology

We employ the linear exponential form of temperature-dependent viscosity:

$$\eta_T^* = \exp\left[\theta(1 - T^*)\right], \tag{1}$$

where η_T^* is nondimensional viscosity (normalized by a reference viscosity η_0 defined at $T^* = 1$), and T^* is nondimensional temperature defined with respect to surface temperature T_S and a temperature scale ΔT:

$$T^* = \frac{T - T_S}{\Delta T}. \tag{2}$$

The parameter θ is the Frank-Kamenetskii parameter, which controls the degree of temperature dependence of viscosity and is related to the activation energy E by

$$\theta = \frac{E\Delta T}{R(T_S + \Delta T)^2}, \tag{3}$$

where R is the universal gas constant. With sufficiently large θ, surface viscosity is high enough to resist convection, forming a stagnant lid. This is the case for values of θ corresponding to silicate mantles. Based on estimates of upper mantle rheological parameters (Karato & Wu, 1993), Earth's mantle likely corresponds to $\theta \sim 20$.

At low temperatures, which lead to extremely large viscosities, the lithosphere deforms in the brittle regime (Kohlstedt et al., 1995). Brittle deformation allows for plate-like behavior on Earth, and it must be accounted for in order to achieve plate tectonics in numerical simulations. Rocks deforming in the brittle regime obey the yield stress criterion, which states that failure occurs when stresses exceed the yield strength τ_Y, generally defined as

$$\tau_Y = c_0 + \mu \rho_0 g z, \tag{4}$$

where c_0 is cohesive strength, μ is friction coefficient, ρ_0 is reference density, g is gravitational acceleration, and z is depth. Brittle deformation is often modeled with an effective viscosity for plastic deformation that obeys the yield stress criterion (Moresi & Solomatov, 1998); this is known as pseudoplastic rheology. For scaling analyses, it is sufficient to treat brittle deformation with pseudoplastic rheology, as opposed to an explicit plastic flow law, as we are concerned with modeling large-scale lithospheric behavior (Moresi & Solomatov, 1998). The effective viscosity for plastic deformation η_Y^* is calculated as

$$\eta_Y^* = \frac{\tau_Y^*}{e_{II}^*}, \tag{5}$$

where τ_Y^* is the nondimensional yield stress and e_{II}^* is the second invariant of the nondimensional strain-rate tensor. The nondimensional yield stress is expressed as

$$\tau_Y^* = c^* + \mu^* z^*. \tag{6}$$

Here, depth z^* is normalized by a length scale D and stress is normalized by $\eta_0 \kappa / D^2$, where κ is thermal diffusivity, such that $c^* = c_0 D^2/(\kappa \eta_0)$ and $\mu^* = \mu \rho_0 g D^3/(\kappa \eta_0)$. By defining the Rayleigh number as

$$Ra = \frac{\alpha \rho_0 g \Delta T D^3}{\kappa \eta_0}, \tag{7}$$

and the nondimensional friction coefficient γ as

$$\gamma = \frac{\mu}{\alpha \Delta T}, \tag{8}$$

where α is thermal expansivity, the nondimensional yield stress criterion may be written as

$$\tau_Y^* = c^* + Ra \gamma z^*. \tag{9}$$

Rock friction experiments at low hydrostatic pressure indicate that cohesive strength is insignificant compared to the friction term (Byerlee, 1978), and we therefore assume $c^* = 10^{-5} Ra\gamma$ in our simulations. The effects of both plastic and ductile deformation are combined by defining fluid viscosity η^* as the harmonic mean of η_T^* and η_Y^*, such that the smaller of the two dominates:

$$\eta^* = \left(\frac{1}{\eta_T^*} + \frac{1}{\eta_Y^*} \right)^{-1}. \tag{10}$$

2.2. Governing Equations

Thermal convection of an incompressible fluid with internal heat generation is governed by the conservation of mass, momentum, and energy, which are represented by the following nondimensional equations, respectively:

$$\nabla \cdot \mathbf{u}^* = 0, \tag{11}$$

$$-\nabla P^* + \nabla \cdot \left[\eta^* \left(\nabla \mathbf{u}^* + \nabla \mathbf{u}^{*T} \right) \right] + Ra T^* \mathbf{e}_z = \mathbf{0}, \tag{12}$$

and

$$\frac{\partial T^*}{\partial t^*} + \mathbf{u}^* \cdot \nabla T^* = \nabla^2 T^* + H^*. \quad (13)$$

Nondimensional time t^* is normalized by the diffusion timescale D^2/κ, and nondimensional velocity $\mathbf{u}^*$ is therefore normalized by κ/D. Nondimensional dynamic pressure P^* is normalized by $\eta_0\kappa/D^2$, and nondimensional heat generation rate per unit mass, H^*, is normalized by $\rho_0 D^2/(k\Delta T)$, where k is thermal conductivity. Viscosity η^* is determined by Equation 10. The unit vector pointing upward is $\mathbf{e}_z$. In the equations of mantle convection, the Rayleigh number Ra signifies the potential vigor of convection.

We consider the general case of the mixed heating mode, wherein the fluid layer is heated from within and from below. This is implemented numerically by imposing temperature boundary conditions at the top and bottom surfaces ($T^* = 0$ at $z^* = 0$ and $T^* = 1$ at $z^* = 1$) along with prescribing the nondimensional internal heating H^*.

All numerical experiments are performed using a finite element code (Korenaga & Jordan, 2003) to solve Equations 11–13 in a 2D Cartesian domain. The domain has an aspect ratio of 4 and is discretized into a grid of 256×64 elements. We impose free-slip boundary conditions. Convection diagnostics are measured on the time-averaged and horizontally averaged temperature, viscosity, and velocity profiles, which are calculated after convection has reached a statistical steady state. We define a statistical steady state as the period after temporal variations in the horizontally averaged surface heat flow drop below 1%. For the demonstration of our scaling analysis (Section 3), we run numerical simulations starting from a linear temperature profile with a perturbation consisting of a sinusoidal component and a random component:

$$T^*(x^*, z^*, t^* = 0) = z^* + 0.2\cos(\pi x^*)\sin(\pi z^*) + \epsilon, \quad (14)$$

where ϵ is randomly selected from $[-1, 1] \times 10^{-3}$. For the application to convective bistability (Section 4), we compare suites of numerical simulations, wherein for a given combination of Ra, H^*, and θ, we either decrease or increase γ and use the results for the previous value of γ as the initial condition. The first simulation in each suite is initialized using Equation 14.

3. Scaling Analysis

3.1. Notes on Convection Mode

In general, thermal convection of a viscous fluid consists of a (nearly) isothermal convecting interior bounded by conducting thermal boundary layers (TBLs). The behavior of the top TBL determines the convection mode. For a given combination of Ra, H^*, and θ, convection mode depends on γ. When γ is sufficiently large, the uppermost part of the top TBL is strong and resists convective instability, resulting in stagnant lid convection. Stagnant lid convection is characterized by an immobile lid overlying the convecting part of the upper TBL, and the interior temperature is relatively high (Figures 1a and 1b). For sufficiently small γ, the entire top TBL is weak enough to be unstable and participate in convection (Figures 1c–1f), resulting in plate tectonic convection. Two regimes of plate tectonic convection may be distinguished. At intermediate values of γ, the aspect ratio of convection cells is large, with downwellings occurring only at the side boundaries (Figure 1d). The convecting interior is homogenous, and the interior temperature is similar to the corresponding stagnant lid case, although the large cold downwellings lead to a lower interior temperature on the horizontally averaged temperature profile (Figures 1c and 1d). At smaller values of γ, aspect ratio of convection cells is relatively small, and nearly the entire fluid layer is comprised of alternating upwellings and downwellings (Figures 1e and 1f). Upwelling occurs via distinct plumes rather than diffuse and passive rising of material. Interior temperature as shown in the horizontally averaged temperature profile decreases with decreasing γ, and it also decreases with depth in the small-γ regime due to the prevalence of upwellings and downwellings (Figure 1e).

Scaling laws for stagnant lid convection (in the mixed heated mode) have been derived by Ferrick and Korenaga (2023) and are independent of γ. We now derive scaling laws for plate tectonic convection. It is important that such scaling laws are consistent with the range of behaviors exhibited within the plate tectonic regime for different values of γ. Numerical simulations presented alongside the scaling analysis are listed in Table 1.

3.2. Scaling Laws for Plate Tectonic Convection

Our scaling approach is based on that introduced by Ferrick and Korenaga (2023), to which we refer readers for detailed descriptions of our approach, its assumptions, and its advantages over previous approaches.

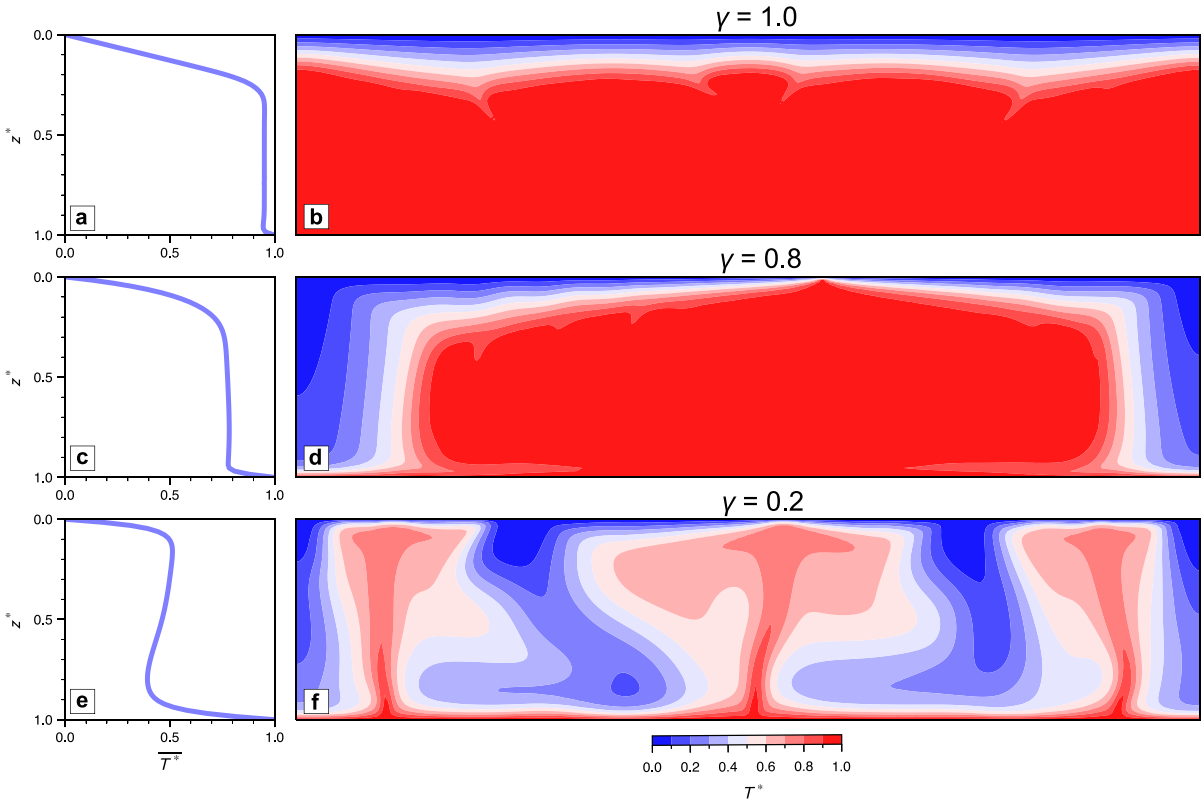

Figure 1. Temperature structure of convection simulations with $Ra = 3 \times 10^8$, $H^* = 0$, $\theta = 21$, and three different values of nondimensional friction coefficient γ: 1.0 (a, b), 0.8 (c, d), and 0.2 (e, f). Leftmost panels show the time-averaged and horizontally averaged temperature $\overline{T^*}$, and rightmost panels show snapshots of the 2D temperature field. The case with $\gamma = 1.0$ is in the stagnant lid regime, and the cases with $\gamma = 0.8$ and $\gamma = 0.2$ are different manifestations of the plate tectonic regime.

The foundation of our approach consists of several basic physical properties of a convecting viscous fluid. The first follows from the conservation of energy, and it states that the surface heat flux is the sum of the basal heat flux and the internal heating:

$$q_t^* = H^* + q_b^* \tag{15}$$

where q_t^* and q_b^* are nondimensional surface and basal heat flux, respectively, and are normalized by $k\Delta T/D$. We may define a Nusselt number for both the top and bottom surfaces (Nu_t and Nu_b, respectively) as the heat flux normalized by a hypothetical conductive heat flux for a system with a temperature contrast ΔT. For mixed heated cases, wherein the temperature contrast is imposed, we simply have $Nu_t = q_t^*$ and $Nu_b = q_b^*$, and Equation 15 may be expressed as

$$Nu_t = H^* + Nu_b \tag{16}$$

The second physical principle employed in our scaling approach is the assumption that the TBLs are conductive, such that heat flow is related to TBL structure by the following:

$$Nu_t = \frac{\Delta T_t^{\mathrm{HF}}}{\delta_t^{\mathrm{HF}}}, \tag{17a}$$

$$Nu_b = \frac{\Delta T_b^{\mathrm{HF}}}{\delta_b^{\mathrm{HF}}}. \tag{17b}$$

Here, ΔT_t^{HF} and ΔT_b^{HF} refer to the nondimensional temperature contrast across the top and bottom TBL, respectively, and δ_t^{HF} and δ_b^{HF} refer to the nondimensional thickness of the top and bottom TBL, respectively. The superscript "HF" denotes the specific definition of the TBLs that is relevant to heat flux; in our previous work, we show

Table 1
Input Parameters (Bold) and Output Measurements of Numerical Simulations With Plate Tectonic Convection

H^*	θ	γ	Nu_t	Nu_b	ΔT_t^{CR}	δ_t^{CR}	ΔT_b^{CR}	δ_b^{CR}
0	**18**	**0.2**	12.02	11.94	0.510	0.258	0.543	0.437
0	**18**	**0.4**	12.71	11.91	0.633	0.341	0.452	0.253
0	**18**	**0.6**	10.73	10.84	0.655	0.295	0.395	0.205
0	**18**	**0.8**	10.02	10.08	0.699	0.292	0.313	0.128
0	**18**	**1.0**	9.61	9.41	0.770	0.343	0.255	0.092
0	**21**	**0.4**	11.10	10.41	0.599	0.437	0.461	0.335
0	**21**	**0.8**	8.08	7.69	0.768	0.367	0.220	0.092
3	**18**	**0.2**	14.66	11.66	0.539	0.204	0.528	0.365
3	**18**	**0.4**	15.79	11.32	0.736	0.298	0.362	0.212
3	**18**	**0.6**	14.73	10.90	0.760	0.300	0.349	0.171
3	**18**	**0.8**	12.28	9.71	0.782	0.263	0.259	0.104
3	**18**	**1.0**	11.77	8.89	0.843	0.317	0.209	0.077
3	**21**	**0.2**	12.73	10.45	0.562	0.272	0.473	0.499
3	**21**	**0.6**	13.53	9.63	0.755	0.441	0.326	0.194
3	**24**	**0.4**	12.95	8.89	0.707	0.370	0.343	0.356
3	**24**	**0.6**	11.69	7.49	0.813	0.338	0.253	0.139
6	**18**	**0.2**	16.93	11.91	0.588	0.163	0.482	0.289
6	**18**	**0.4**	18.64	11.48	0.758	0.302	0.354	0.199
6	**18**	**0.6**	18.24	10.95	0.801	0.283	0.328	0.162
6	**18**	**0.8**	16.27	10.11	0.845	0.256	0.275	0.113
6	**21**	**0.4**	17.25	9.93	0.757	0.323	0.346	0.246
6	**21**	**0.6**	15.92	9.44	0.812	0.278	0.305	0.174
6	**24**	**0.2**	14.40	8.63	0.593	0.279	0.456	0.499

Note. For all cases, $Ra = 3 \times 10^8$.

that there are several ways of defining TBLs, and it is important to identify which definition applies to a given equation used in the scaling derivation (Ferrick & Korenaga, 2023).

The third governing principle is the boundary layer stability criterion, which states that a TBL grows until it reaches instability and breaks off as an upwelling or downwelling (Howard, 1966). In other words, TBLs are at a steady state with respect to marginal stability and can be described by a stability criterion (i.e., a critical Rayleigh number). We have previously demonstrated the validity of the boundary layer stability criterion for mixed heated convection (Ferrick & Korenaga, 2023). This criterion is expressed by defining a local Rayleigh number for each TBL and equating it to a critical Rayleigh number Ra_{cr}:

$$Ra_{cr} = \frac{Ra\Delta T_t^{CR}\left(\delta_t^{CR}\right)^3}{\eta_t} = \frac{Ra\Delta T_b^{CR}\left(\delta_b^{CR}\right)^3}{\eta_b}. \quad (18)$$

Here, the superscript "CR" refers to the TBL definition relevant for instability, and η_t and η_b are representative nondimensional viscosities for the top and bottom TBL, respectively. Because the top TBL generally has a well-defined maximum viscosity (Figure 2), we choose to define η_t as the maximum viscosity within the top TBL. For consistency, we define η_b analogously as the maximum viscosity within the bottom TBL. We will later seek scaling laws to relate η_t and η_b to other convective parameters.

We measure TBL parameters relevant to instability by calculating local Rayleigh number Ra_{TBL} as a function of TBL thickness. For example, local Rayleigh number for the top TBL is calculated at a given depth Z as

$$Ra_{\mathrm{TBL},t}(Z) = \frac{Ra\,\overline{T^*}(z^* = Z)Z^3}{\max\left[\overline{\eta^*}(z^* \le Z)\right]}, \quad (19)$$

where $\overline{T^*}$ and $\overline{\eta^*}$ are the time-averaged and horizontally averaged temperature and viscosity profiles, respectively. The parameters δ_t^{CR}, ΔT_t^{CR}, and η_t are defined according to where $Ra_{\mathrm{TBL},t}$ surpasses a critical Rayleigh number (Figure 2a). We assume $Ra_{cr} = 500$, which generally produces TBLs consistent with the boundary between the conducting region and the convecting interior. To obtain measurements of δ^{HF} and ΔT^{HF} such that Equation 17 is satisfied, we impose

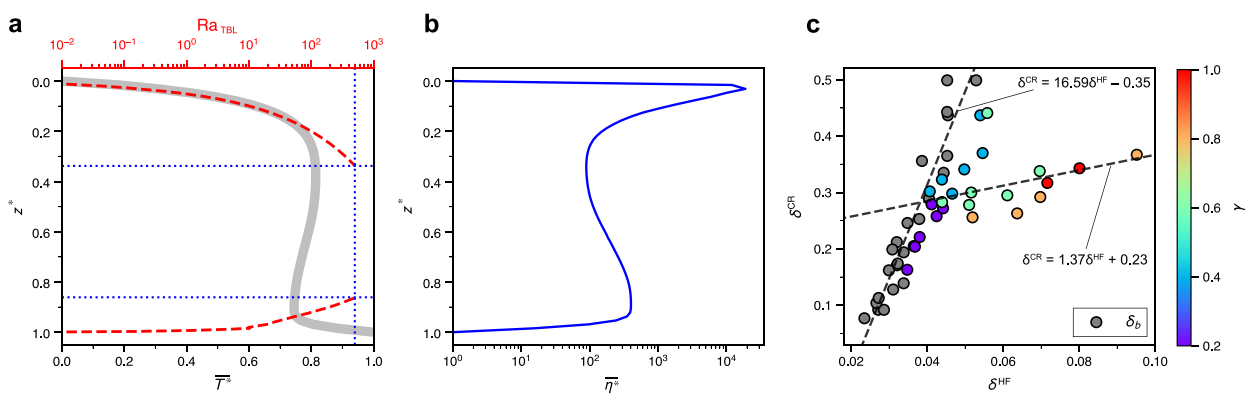

Figure 2. Measurement of thermal boundary layer (TBL) properties. Panel (a) demonstrates the method of measuring ΔT^{CR}, δ^{HF}, and TBL viscosity; panel (b) shows the time-averaged and horizontally averaged viscosity profile used in the measurement shown by panel (a); and panel (c) shows the relationship between the two definitions of TBL thickness. For panels (a) and (b), the example shown corresponds to $Ra = 3 \times 10^8$, $H^* = 3$, $\theta = 24$, and $\gamma = 0.6$.

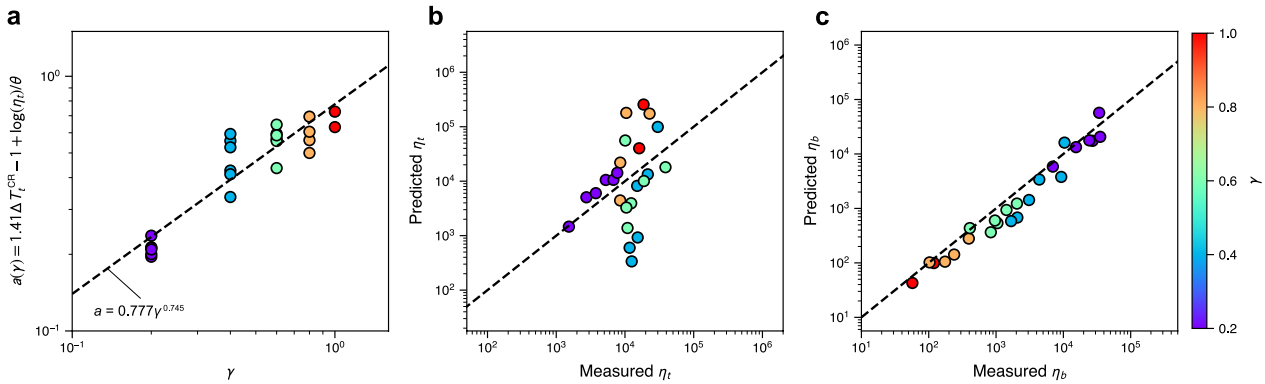

Figure 3. Comparison of the scaling relationships for η_t and η_b with measured values. Panel (a) shows the fit to the γ-dependence of η_t. Panel (b) shows the fit to the full scaling for η_t. Panel (c) shows the fit for η_b. Symbol color corresponds to nondimensional friction coefficient γ.

$$\Delta T_t^{\mathrm{HF}} = \Delta T_t^{\mathrm{CR}}, \tag{20a}$$

$$\Delta T_b^{\mathrm{HF}} = \Delta T_b^{\mathrm{CR}}, \tag{20b}$$

and we then determine TBL thickness from the measured heat flux, so that $\delta_t^{\mathrm{HF}} = \Delta T_t^{\mathrm{HF}}/Nu_t$ and $\delta_b^{\mathrm{HF}} = \Delta T_b^{\mathrm{HF}}/Nu_b$. Prescribing equality of ΔT^{HF} and ΔT^{CR} means that the relationship between the two TBL definitions is entirely described by the relationship between δ^{HF} and δ^{CR}, thereby consolidating the number of fitting parameters. Figure 2c shows that the measured values of δ^{HF} and δ^{CR} are linearly related, so that we may assume

$$\delta_t^{\mathrm{HF}} = c_1\delta_t^{\mathrm{CR}} + c_2, \tag{21a}$$

$$\delta_b^{\mathrm{HF}} = c_3\delta_b^{\mathrm{CR}} + c_4, \tag{21b}$$

where the c_i are constants. We find that, for the bottom TBL, the best fit parameters are $c_3 = 16.59$ and $c_4 = -0.35$, while the parameters for the top TBL fall into two distinct regimes (Figure 2c). For $\gamma \lesssim 0.6$, the trend coincides with that of the bottom TBL: $c_1 = 16.59$ and $c_2 = -0.35$. This makes intuitive sense, because the bottom TBL is always dominated by temperature-dependent viscosity, but the top TBL will only be dominated by temperature-dependent viscosity at sufficiently low γ. For $\gamma \gtrsim 0.6$, the best fit parameters are $c_1 = 1.37$ and $c_2 = 0.23$. For these cases, the top TBL is likely influenced by plastic deformation.

We now turn to scaling relationships for η_t and η_b. Korenaga (2010b) found that the viscosity contrast between the top TBL and the convecting interior depends only on θ and γ:

$$\eta_t/\eta_i = \exp[(a_1\gamma^{a_2})\theta]. \tag{22}$$

Assuming that plastic deformation may be ignored within the convecting interior, we may assume interior viscosity scales as $\eta_i = \exp\left[\theta\left(1 - \beta\Delta T_t^{\mathrm{CR}}\right)\right]$, where we assume interior temperature scales with ΔT_t^{CR}. We may therefore parameterize η_t as

$$\eta_t = \exp\left[(a_1\gamma^{a_2})\theta + \theta\left(1 - \beta\Delta T_t^{\mathrm{CR}}\right)\right]. \tag{23}$$

We solve for the best fit parameters simultaneously, which yields $a_1 = 0.777$, $a_2 = 0.745$, and $\beta = 1.41$ (Figures 3a and 3b). This phenomenological scaling for η_t does not conform to our physics-based scaling approach; it will be the task of future studies to derive a scaling for η_t from physical principles. The scaling for η_b is more straightforward, as the bottom TBL is simply governed by temperature-dependent viscosity alone due to its high temperature. We may assume that η_b obeys the linear exponential equation for viscosity:

$$\eta_b = \exp\left[\theta\Delta T_b^{\mathrm{CR}}\right]. \tag{24}$$

Because we have measured the bottom TBL using its maximum viscosity (Equation 19), we have assumed in Equation 24 that the temperature at the top of the bottom TBL (i.e., its lowest temperature) is relevant for the scaling. This scaling yields an excellent fit to the numerical measurements (Figure 3c).

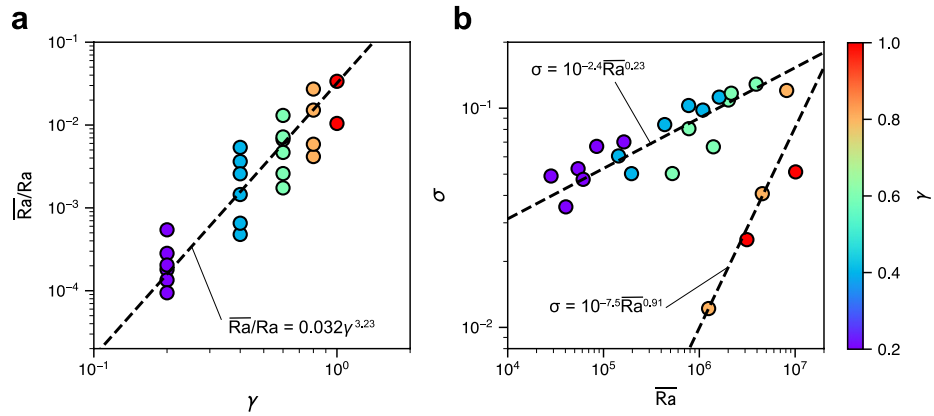

Figure 4. Comparison of the scaling for temperature overshoot σ with numerical measurements. Panel (a) shows the relationship between effective Rayleigh number and γ, and panel (b) shows the relationship between σ and effective Rayleigh number. Symbol color corresponds to nondimensional friction coefficient γ.

The fourth and final physical constraint comes from the assumption that the convecting interior is roughly isothermal, and thus the temperature contrasts across the TBLs sum to a constant:

$$\Delta T_t^{\mathrm{CR}} + \Delta T_b^{\mathrm{CR}} = 1 + \sigma. \tag{25}$$

Here, σ is the so-called temperature overshoot previously introduced for isoviscous convection (Ferrick & Korenaga, 2023); σ is needed because the interior is not perfectly isothermal. This results from interactions of upwellings and downwellings with TBLs. For example, when a cold downwelling descends, it does not necessarily equilibrate with the internal temperature, so that when it reaches the bottom TBL it decreases the horizontally averaged temperature near the boundary of the bottom TBL. We have previously demonstrated two competing controls on the magnitude of σ (Ferrick & Korenaga, 2023). When convection increases in vigor, TBLs become thinner, thereby reducing their potential to perturb the thermal structure of the opposite TBL, but convection speeds increase, thereby decreasing the time available for upwellings and downwellings to equilibrate with the internal temperature. These effects can be parameterized as a function of the effective Rayleigh number $\overline{Ra}$, which represents the vigor of convection and is defined as Ra divided by the log-average of the time-averaged and horizontally averaged viscosity profile. We find that the dependence of σ on $\overline{Ra}$ again falls into two regimes, with a transition at $\gamma \sim 0.6$ (Figure 4b). The best fit functions for the two regimes are as follows:

$$\sigma|_{\gamma \le 0.6} = 10^{-2.4}\overline{Ra}^{0.23}, \tag{26a}$$

$$\sigma|_{\gamma > 0.6} = 10^{-7.5}\overline{Ra}^{0.91}. \tag{26b}$$

Effective Rayleigh number is most simply represented as a function of gamma (Figure 4a) with the following best fit parameters:

$$\overline{Ra}/Ra = 0.032\gamma^{3.23}. \tag{27}$$

These four physical principles constitute a full set of scaling equations. For example, combining Equations 16–18, 20, 21[16–18], and 25 gives

$$\frac{c_1 \Delta T_t^{\mathrm{HF}}}{\left(Ra_{cr}\eta_t/Ra\Delta T_t^{\mathrm{HF}}\right)^{1/3} - c_2} = H^* + \frac{c_3\left(1 + \sigma - \Delta T_t^{\mathrm{HF}}\right)}{\left(Ra_{cr}\eta_b/Ra\left(1 + \sigma - \Delta T_t^{\mathrm{HF}}\right)\right)^{1/3} - c_4}. \tag{28}$$

Substituting the appropriate scalings for η_t, η_b, and σ (Equations 23, 24, 26, and 27) leaves ΔT_t^{HF} as the only unknown quantity in Equation 28. Equation 28 must be solved numerically, rather than explicitly, for ΔT_t^{HF}. After solving for ΔT_t^{HF}, the scaling equations may be used to solve for other quantities such as surface heat flow. Upon comparison with numerical experiments, the scaling laws predict convective properties relatively well

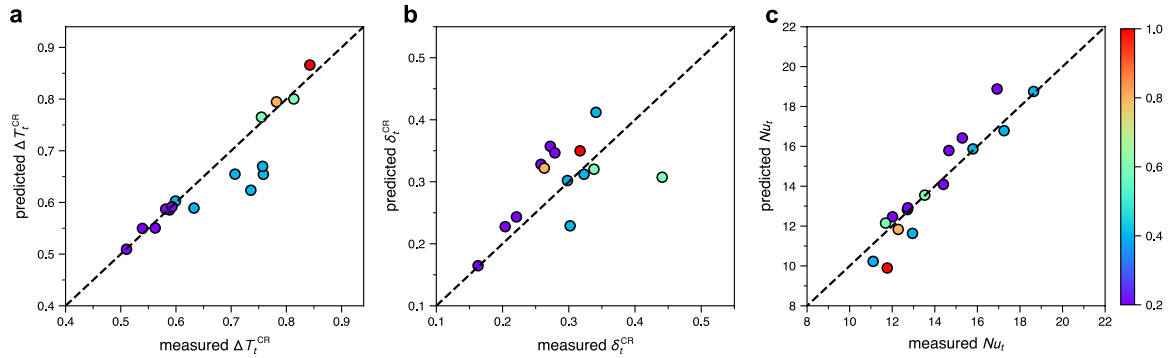

Figure 5. Final scaling results for plate tectonic convection with mixed heating. Panels (a–c) compare the measured and predicted values of, respectively, the temperature change across the top thermal boundary layer (TBL), the thickness of the top TBL, and surface heat flux. Symbol color corresponds to nondimensional friction coefficient γ.

(Figure 5), considering the increased complexity compared to the isoviscous and purely temperature-dependent viscosity cases (Ferrick & Korenaga, 2023). The greatest source of uncertainty is the top TBL viscosity, for which a physically justified scaling is still needed (see Figure S1 in Supporting Information S1 for scaling predictions when η_t is perfectly known).

4. Implications for the Bistability of Convection Mode

In numerical simulations, convection mode can depend on the prescribed initial conditions (e.g., Noack & Breuer, 2014; Weller & Lenardic, 2012). What this means for tectonic mode on planets is not immediately obvious, but a popular interpretation is that knowledge of planetary evolution is required to predict tectonic mode (Lenardic & Crowley, 2012; Noack & Breuer, 2014; Weller et al., 2015; Weller & Lenardic, 2012). Figure 6 presents pairs of simulation suites with different initial conditions (see also Table S1 in Supporting Information S1). For a given combination of H^* and θ, we run one set of simulations in which γ is incrementally increased from 0.2 to 1.0, and another set in which γ is incrementally decreased from 1.0 to 0.2. As γ changes, so does

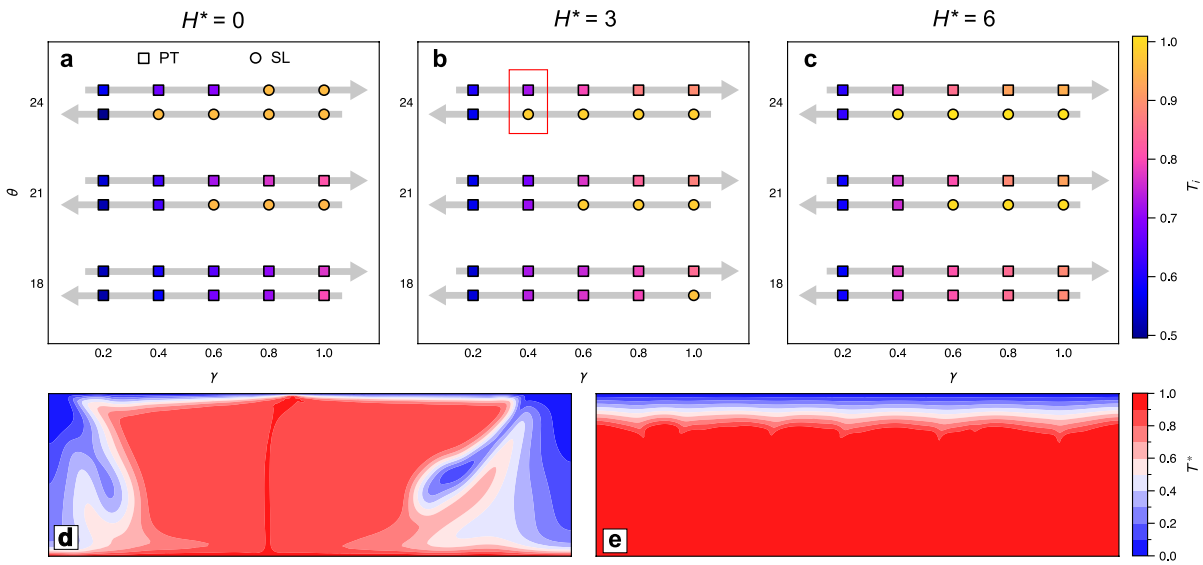

Figure 6. Results of numerical simulation suites. For each suite of runs (denoted by the gray arrows), nondimensional friction coefficient γ is either increased or decreased between simulations. Each simulation is initialized from the steady state result of the previous simulation. For all cases, $Ra = 3 \times 10^8$. Panels (a–c) comprise a convective regime diagram. Square symbols indicate plate tectonics; circular symbols indicate stagnant lid. Symbol color refers to the internal temperature T_i, defined here as the midpoint temperature of the time-average and horizontally averaged temperature profile. Panels (d) and (e) show temperature snapshots of the plate tectonic and stagnant lid simulations, respectively, outlined in (b).

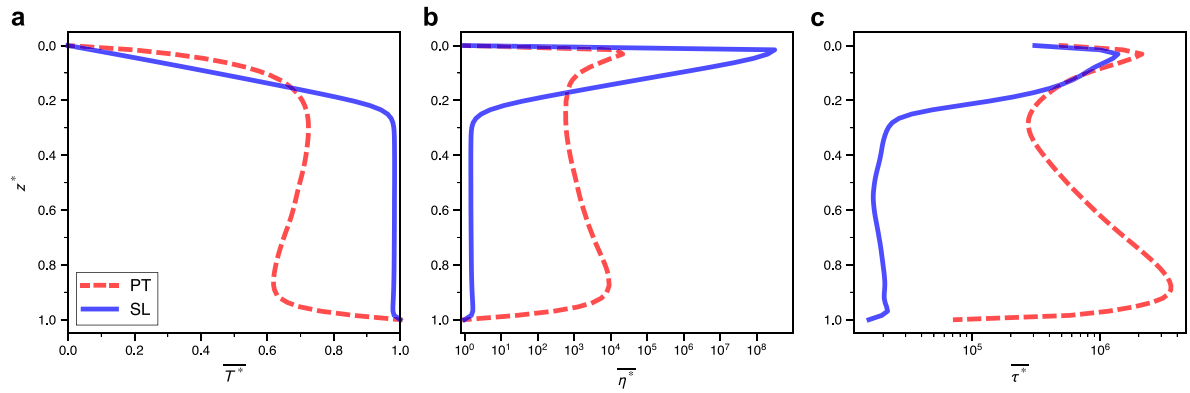

Figure 7. Comparison of the two stable tectonic states for the following input parameters: $Ra = 3 \times 10^8$, $H^* = 3$, $\theta = 24$, and γ. Panels (a–c) present nondimensional time-averaged and horizontally averaged temperature, viscosity, and stress, respectively. Dashed red and solid blue curves correspond to the plate tectonic (PT) and stagnant lid (SL) case, respectively.

tectonic mode, internal temperature, and other convective properties. Two cases with the same nondimensional input parameters may have different convection modes if one case starts from an initially plate tectonic state and the other starts from an initially stagnant lid state. More specifically, tectonic mode appears to have a "stickiness" that is characteristic of hysteresis: convection starting from a stagnant lid state tends to remain in a stagnant lid state, and convection starting from a plate tectonic state tends to remain in a plate tectonic state. As a result, for at least part of the (nondimensional) parameter space there are two stable tectonic regimes.

Upon first consideration, it may seem surprising that two simulations with the same nondimensional input parameters can exhibit different tectonic modes. It may also seem troubling, because requiring knowledge of planetary history would encumber the prediction of tectonic mode. However, two fundamental differences between simulations with opposing tectonic mode can dispel these concerns: (a) different nondimensional internal temperature, resulting in different rheological setting, and (b) different heating mode, resulting in different convective stresses.

Regarding the first statement, plate tectonic convection exhibits (often much) lower internal temperatures than stagnant lid convection corresponding to the same nondimensional model parameters (Figure 6). As an example, consider the two cases with opposing tectonic modes corresponding to $Ra = 3 \times 10^8$, $H^* = 3$, $\theta = 24$, and $\gamma = 0.4$. The plate tectonic case and the stagnant lid case exhibit nondimensional internal temperatures of ~0.7 and ~0.98, respectively (Figures 6 and 7a). As a result of different internal temperatures, the viscosity contrast across the lithosphere is roughly six orders of magnitude larger in the stagnant lid case (Figure 7b). Further, although the two cases share the same θ and γ, they have very different rheological parameters upon dimensionalization. This is not immediately obvious due to how θ and γ are conventionally defined. The Frank-Kamenetskii parameter θ has traditionally been used to investigate stagnant lid convection with purely internal heating (e.g., Solomatov & Moresi, 2000), in which the total temperature contrast ΔT is always the internal temperature T_i. Thus, $\exp(\theta)$ corresponds to the viscosity contrast across the top TBL. Therefore, a proper treatment of mixed heating requires relating θ and E, as well as γ and μ, by the dimensional internal temperature. In other words, Equations 3 and 8 should be rescaled by T_i when converting to dimensional parameters. Applying this reasoning to the above example, and assuming $T_S = 273$ K, $\Delta T = 1{,}900$ K, and $\alpha = 2 \times 10^{-5}$ K^{-1}, the plate tectonic case corresponds to $E \sim 390$ kJ/mol and $\mu \sim 0.011$, whereas the stagnant lid case corresponds to $E \sim 490$ kJ/mol and $\mu \sim 0.015$. Thus, although a unique combination of nondimensional model parameters may exhibit two stable tectonic states, these states do not correspond to identical rheological conditions. The lithosphere in plate tectonic convection is weaker than that in stagnant lid convection corresponding to the same nondimensional model parameters.

The second significant difference between simulations with opposing tectonic states is heating mode. With respect to the pair of simulations introduced above, the plate tectonic and stagnant lid cases have internal heating ratios of 0.24 and 0.66, respectively, where the internal heating ratio is defined as H^*/q_t^*. Heating mode, and to a much smaller extent internal temperature, control convective stresses, such that convective stresses increase with decreasing internal heating ratio (i.e., increasing contribution from the bottom TBL) and decreasing internal temperature (Korenaga, 2017). As a result of this effect, the base of the top TBL in the plate tectonic case experiences higher stresses than that corresponding to the stagnant lid case (Figure 7c).

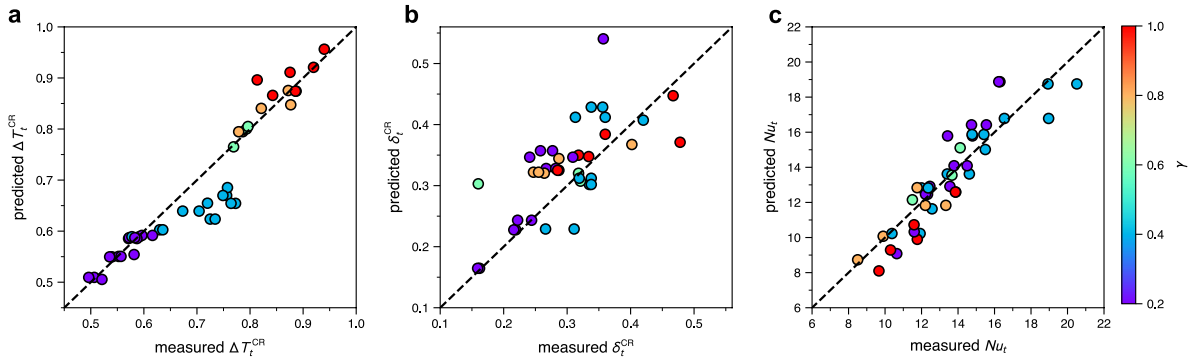

Figure 8. Scaling laws for plate tectonic convection with mixed heating applied to the plate tectonic cases in Figure 6. Panels (a–c) compare the measured and predicted values of, respectively, the temperature change across the top thermal boundary layer (TBL), the thickness of the top TBL, and surface heat flux. Symbol color corresponds to the nondimensional friction coefficient γ.

Considering together the effects of nondimensional internal temperature and heating mode, confidence can be restored in the prospect of predicting tectonic mode from planetary properties. Even when a unique combination of the conventional nondimensional model parameters (Ra, H^*, θ, and γ) exhibits two stable tectonic states, these two states correspond to vastly different rheological scenarios. In one case, the lithosphere is moderately stronger than the convecting interior, and in the other, it is significantly stronger (Figure 7). Indeed, the two scenarios correspond to fundamentally different mantle rheologies—that is, different viscoplastic properties of mantle rocks. Due to the effect of nondimensionalization, this may not be not immediately clear. It may appear that two simulations with identical nondimensional rheological parameters have identical rheological settings, but, as we have shown, the same nondimensional input parameters do not guarantee the same combination of activation energy and friction coefficient. Thus, the appearance of multiple stable states in numerical simulations (Lenardic & Crowley, 2012; Noack & Breuer, 2014; Weller et al., 2015; Weller & Lenardic, 2012) is fully consistent with the notion that for a given combination of rheological parameters (i.e., activation energy and friction coefficient) and heating mode, tectonic mode is unique.

Our scaling analyses are able to describe convective properties regardless of tectonic mode, as we have generalized our approach for both stagnant lid convection and plate tectonic convection. When compared to the simulations used in Section 3.2 to derive the scaling laws, the plate tectonic cases in Figure 6 yield a similar fit to scaling predictions of TBL thickness, TBL viscosity, and temperature overshoot (compare Figures 2–4 with Figures S2–S4 in Supporting Information S1). We apply our plate tectonics scaling laws (Equation 28) to these cases, and to the stagnant lid cases we apply the scaling equations relevant to purely temperature-dependent viscosity (Equations 45 and 46 in Ferrick and Korenaga (2023)). The scaling predictions are successful (Figures 8 and 9). Figure 8 indicates that, for the plate tectonic cases, Equation 28 predicts heat flux and top TBL properties (thickness and temperature change) with accuracy comparable to that corresponding to the cases starting from a quasi-linear temperature profile (Figure 5). Figure 9 indicates that the scaling derived in Ferrick and Korenaga (2023) predicts heat flux, TBL properties, and stagnant lid properties with a high degree of accuracy. The scaling for stagnant lid convection is generally more accurate than that for plate tectonic convection (compare Figures 8 and 9). The success of our scaling laws confirms that, regardless of initial conditions, steady state convective parameters such as internal temperature and surface heat flux may be accurately predicted when tectonic mode is known. And, as we have demonstrated, tectonic mode can be distinguished for any set of rheological parameters as long as ΔT and T_i are known.

5. Conclusions

In general, planetary mantles are heated both from within and from below, and they deform in both the plastic and viscous regimes depending on temperature and pressure. However, scaling laws accommodating both mixed heating and pseudoplastic rheology have previously remained unaddressed. We have extended our physics-based scaling approach to mixed heated convection with pseudoplastic rheology. These scaling laws are the first to be fully applicable to planetary mantles, as they have been generalized for the appropriate heating mode and rheology. Fine-tuning of several components will improve the accuracy, as well as our physical understanding, of the

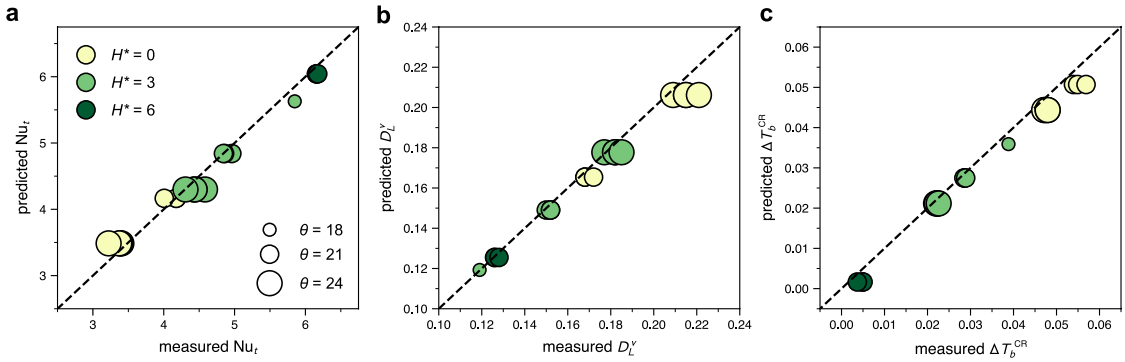

Figure 9. Scaling laws for stagnant lid convection with mixed heating applied to the stagnant lid cases in Figure 6. Panels (a–c) compare the measured and predicted values of, respectively, the surface heat flux, the thickness of the stagnant lid D_L^v (defined in Ferrick and Korenaga (2023)), and the temperature change across the bottom thermal boundary layer (TBL). Symbol color corresponds to nondimensional internal heating H^*, and symbol size corresponds to the Frank-Kamenetskii parameter θ.

scaling equations. For one, a physics-based characterization of lithospheric viscosity is still needed; Equation 23 is a phenomenological scaling for η_t inferred from numerical results. Additionally, we identify two different regimes of plate tectonic behavior with a transition at $\gamma \sim 0.6$ (see e.g., Figures 1c–1f, 2c[1c–1f], and 4b). Understanding the origin of this transition, and the dynamical differences between the two regimes, will guide the improvement of the scaling equations describing each of the two regimes.

We have applied our scaling laws for stagnant lid convection (Ferrick & Korenaga, 2023) and plate tectonic convection to numerical simulations exhibiting so-called bistability, wherein convection mode depends on the prescribed initial conditions. The success of the scaling laws indicates that steady-state convective properties may be accurately predicted for a given tectonic mode, regardless of initial conditions. Further, by clarifying issues such as heating mode and nondimensionalization, we have demonstrated that tectonic mode is unique with respect to dimensional planetary properties, despite the apparent bistability of numerical simulations. We thereby affirm the feasibility of predicting tectonic mode and convective behavior from first-order planetary properties—a fundamental task for thermal evolution modeling—without the need for modeling planetary history as suggested in recent years. Previous scaling analysis has shown that tectonic mode uniquely depends on rheological setting (i.e., temperature contrast across the top TBL) and internal convective vigor represented by the internal Rayleigh number (Korenaga, 2010b). We therefore suggest that efforts to predict tectonic mode should proceed by scaling rheological parameters (e.g., activation energy and friction coefficient) and internal convective vigor as functions of fundamental planetary properties.

Data Availability Statement

This work is theoretical in nature and may be reproduced from the details provided in the main text. All numerical data are presented in Table 1 and Table S1 (Supporting Information S1) and may be accessed directly at https://doi.org/10.17632/8ptxb4dh7v.1 (Ferrick, 2023).

Acknowledgments
This research was supported in part by the U.S. National Science Foundation Grant EAR-2102777 (J.K.) and the U.S. National Aeronautics and Space Administration under Cooperative Agreement 80NSSC19M0069 issued through the Science Mission Directorate (J.K.). The authors thank Thomas Duvernay and one anonymous reviewer for constructive and insightful reviews.

References

Bercovici, D. (1993). A simple model of plate generation from mantle flow. *Geophysical Journal International*, *114*(3), 635–650. https://doi.org/10.1111/j.1365-246X.1993.tb06993.x

Byerlee, J. (1978). Friction of rocks. In J. D. Byerlee & M. Wyss (Eds.), *Rock friction and Earthquake prediction* (pp. 615–626). Birkhäuser. https://doi.org/10.1007/978-3-0348-7182-2_4

Choblet, G. (2012). On the scaling of heat transfer for mixed heating convection in a spherical shell. *Physics of the Earth and Planetary Interiors*, *206–207*, 31–42. https://doi.org/10.1016/j.pepi.2012.06.007

Christensen, U. R. (1985). Heat transport by variable viscosity convection II: Pressure influence, non-Newtonian rheology and decaying heat sources. *Physics of the Earth and Planetary Interiors*, *37*(2), 183–205. https://doi.org/10.1016/0031-9201(85)90051-2

Ferrick, A. (2023). Data for: Scaling laws for mixed heated convection with pseudoplastic rheology: Implications for bistability of convection mode. *Mendeley Data. (V1)*. https://doi.org/10.17632/8ptxb4dh7v.1

Ferrick, A. L., & Korenaga, J. (2023). Generalizing scaling laws for mantle convection with mixed heating. *Journal of Geophysical Research: Solid Earth*, *128*, e2023JB026398. https://doi.org/10.1029/2023JB026398

Foley, B. J., & Bercovici, D. (2014). Scaling laws for convection with temperature-dependent viscosity and grain-damage. *Geophysical Journal International*, *199*(1), 580–603. https://doi.org/10.1093/gji/ggu275

Grigné, C., Labrosse, S., & Tackley, P. J. (2005). Convective heat transfer as a function of wavelength: Implications for the cooling of the Earth. *Journal of Geophysical Research*, *110*, B03409. https://doi.org/10.1029/2004JB003376

Gurnis, M. (1989). A reassessment of the heat transport by variable viscosity convection with plates and lids. *Geophysical Research Letters*, *16*(2), 179–182. https://doi.org/10.1029/GL016i002p00179

Howard, L. N. (1966). Convection at high Rayleigh number. In H. Görtler (Ed.), *Applied mechanics* (pp. 1109–1115). Springer. https://doi.org/10.1007/978-3-662-29364-5_147

Karato, S.-I., & Wu, P. (1993). Rheology of the upper mantle: A synthesis. *Science*, *260*(5109), 771–778. https://doi.org/10.1126/science.260.5109.771

Kohlstedt, D. L., Evans, B., & Mackwell, S. J. (1995). Strength of the lithosphere: Constraints imposed by laboratory experiments. *Journal of Geophysical Research*, *100*(B9), 17587–17602. https://doi.org/10.1029/95JB01460

Korenaga, J. (2010a). On the likelihood of plate tectonics on super-earths: Does size matter? *The Astrophysical Journal Letters*, *725*(1), L43–L46. https://doi.org/10.1088/2041-8205/725/1/L43

Korenaga, J. (2010b). Scaling of plate tectonic convection with pseudoplastic rheology. *Journal of Geophysical Research*, *115*, B11405. https://doi.org/10.1029/2010JB007670

Korenaga, J. (2017). Pitfalls in modeling mantle convection with internal heat production. *Journal of Geophysical Research: Solid Earth*, *122*, 4064–4085. https://doi.org/10.1002/2016JB013850

Korenaga, J. (2020). Plate tectonics and surface environment: Role of the oceanic upper mantle. *Earth-Science Reviews*, *205*, 103185. https://doi.org/10.1016/j.earscirev.2020.103185

Korenaga, J., & Jordan, T. H. (2003). Physics of multiscale convection in Earth's mantle: Onset of sublithospheric convection. *Journal of Geophysical Research*, *108*(B7), 2333. https://doi.org/10.1029/2002JB001760

Lenardic, A., & Crowley, J. W. (2012). On the notion of well-defined tectonic regimes for terrestrial planets in this solar system and others. *The Astrophysical Journal*, *755*(2), 132. https://doi.org/10.1088/0004-637X/755/2/132

Lenardic, A., Crowley, J., Jellinek, A., & Weller, M. (2016). The solar system of forking paths: Bifurcations in planetary evolution and the search for life-bearing planets in our galaxy. *Astrobiology*, *16*(7), 551–559. https://doi.org/10.1089/ast.2015.1378

Lourenço, D. L., Rozel, A., & Tackley, P. J. (2016). Melting-induced crustal production helps plate tectonics on Earth-like planets. *Earth and Planetary Science Letters*, *439*, 18–28. https://doi.org/10.1016/j.epsl.2016.01.024

Lowman, J. P., King, S. D., & Gable, C. W. (2001). The influence of tectonic plates on mantle convection patterns, temperature and heat flow. *Geophysical Journal International*, *146*(3), 619–636. https://doi.org/10.1046/j.1365-246X.2001.00471.x

Monnereau, M., & Quéré, S. (2001). Spherical shell models of mantle convection with tectonic plates. *Earth and Planetary Science Letters*, *184*(3–4), 575–587. https://doi.org/10.1016/S0012-821X(00)00334-4

Moresi, L., & Solomatov, V. (1998). Mantle convection with a brittle lithosphere: Thoughts on the global tectonic styles of the Earth and Venus. *Geophysical Journal International*, *133*(3), 669–682. https://doi.org/10.1046/j.1365-246X.1998.00521.x

Noack, L., & Breuer, D. (2014). Plate tectonics on rocky exoplanets: Influence of initial conditions and mantle rheology. *Planetary and Space Science*, *98*, 41–49. https://doi.org/10.1016/j.pss.2013.06.020

O'Neill, C., & Lenardic, A. (2007). Geological consequences of super-sized Earths. *Geophysical Research Letters*, *34*, L19204. https://doi.org/10.1029/2007GL030598

O'Neill, C., Lenardic, A., Weller, M., Moresi, L., Quenette, S., & Zhang, S. (2016). A window for plate tectonics in terrestrial planet evolution? *Physics of the Earth and Planetary Interiors*, *255*, 80–92. https://doi.org/10.1016/j.pepi.2016.04.002

Solomatov, V. S., & Moresi, L.-N. (2000). Scaling of time-dependent stagnant lid convection: Application to small-scale convection on Earth and other terrestrial planets. *Journal of Geophysical Research*, *105*(B9), 21795–21817. https://doi.org/10.1029/2000JB900197

Stein, C., Finnenkötter, A., Lowman, J. P., & Hansen, U. (2011). The pressure-weakening effect in super-Earths: Consequences of a decrease in lower mantle viscosity on surface dynamics. *Geophysical Research Letters*, *38*, L21201. https://doi.org/10.1029/2011GL049341

Tackley, P. J. (1998). Self-consistent generation of tectonic plates in three-dimensional mantle convection. *Earth and Planetary Science Letters*, *157*(1), 9–22. https://doi.org/10.1016/S0012-821X(98)00029-6

Valencia, D., & O'Connell, R. J. (2009). Convection scaling and subduction on Earth and super-Earths. *Earth and Planetary Science Letters*, *286*(3), 492–502. https://doi.org/10.1016/j.epsl.2009.07.015

Valencia, D., O'Connell, R. J., & Sasselov, D. D. (2007). Inevitability of plate tectonics on super-Earths. *The Astrophysical Journal*, *670*(1), L45–L48. https://doi.org/10.1086/524012

Van Heck, H. J., & Tackley, P. J. (2011). Plate tectonics on super-Earths: Equally or more likely than on Earth. *Earth and Planetary Science Letters*, *310*(3), 252–261. https://doi.org/10.1016/j.epsl.2011.07.029

Weller, M. B., & Lenardic, A. (2012). Hysteresis in mantle convection: Plate tectonics systems. *Geophysical Research Letters*, *39*, L10202. https://doi.org/10.1029/2012GL051232

Weller, M. B., Lenardic, A., & O'Neill, C. (2015). The effects of internal heating and large scale climate variations on tectonic bi-stability in terrestrial planets. *Earth and Planetary Science Letters*, *420*, 85–94. https://doi.org/10.1016/j.epsl.2015.03.021

Wong, T., & Solomatov, V. S. (2015). Towards scaling laws for subduction initiation on terrestrial planets: Constraints from two-dimensional steady-state convection simulations. *Progress in Earth and Planetary Science*, *2*(1), 18. https://doi.org/10.1186/s40645-015-0041-x

Zhong, S., Zuber, M. T., Moresi, L., & Gurnis, M. (2000). Role of temperature-dependent viscosity and surface plates in spherical shell models of mantle convection. *Journal of Geophysical Research*, *105*(B5), 11063–11082. https://doi.org/10.1029/2000JB900003